Mediterranean Land Use and Land Cover Classification Assessment Using High Spatial Resolution Data

Mohamed Elhag [1], Silvena Boteva [2]

[1] Department of Hydrology and Water Resources Management, Faculty of Meteorology, Environment & Arid Land Agriculture, King Abdulaziz University Jeddah, 21589, Kingdom of Saudi Arabia
[2] Department of Ecology and Environmental Protection, Faculty of Biology, Sofia University, Sofia, 1164, Bulgaria

E-mail: melhag@kau.edu.sa

Abstract. Landscape fragmentation is noticeably practiced in Mediterranean regions and imposes substantial complications in several satellite image classification methods. To some extent, high spatial resolution data were able to overcome such complications. For better classification performances in Land Use Land Cover (LULC) mapping, the current research adopts different classification methods comparison for LULC mapping using Sentinel-2 satellite as a source of high spatial resolution. Both of pixel-based and an object-based classification algorithms were assessed; the pixel-based approach employs Maximum Likelihood (ML), Artificial Neural Network (ANN) algorithms, Support Vector Machine (SVM), and, the object-based classification uses the Nearest Neighbour (NN) classifier. Stratified Masking Process (SMP) that integrates a ranking process within the classes based on spectral fluctuation of the sum of the training and testing sites was implemented. An analysis of the overall and individual accuracy of the classification results of all four methods reveals that the SVM classifier was the most efficient overall by distinguishing most of the classes with the highest accuracy. NN succeeded to deal with artificial surface classes in general while agriculture area classes, and forest and semi-natural area classes were segregated successfully with SVM. Furthermore, a comparative analysis indicates that the conventional classification method yielded better accuracy results than the SMP method overall with both classifiers used, ML and SVM.

1. Introduction

Several remote sensing scholarly works have used multispectral remotely sensed imagery to provide additional data, which prove to be a valuable source of spatio-temporal data for several applications. Widely used applications are: land covers classification, detection of archaeological cropmarks, spatial features extraction and classification in residential areas, road extraction, estimation of urban expansion, automated mapping of stream features, classification and transportation feature extraction, mapping snow cover and evaluation of geomorphological features [1, 2].

Content from this work may be used under the terms of the Creative Commons Attribution 3.0 licence. Any further distribution of this work must maintain attribution to the author(s) and the title of the work, journal citation and DOI.
Published under licence by IOP Publishing Ltd

Urban Spatial Features extraction and classification were investigated in urban areas by Huang et al. [3] using high spatial resolution multispectral imagery. Quick bird datasets was used. Principally, Structural Feature Set (SFS) was anticipated to examine statistically the direction-lines histogram features of. Dimension reduction was applied to avoid information redundancy. Then, four stochastic classifiers were tested to evaluate SFS and other spatial feature sets. They found that the implemented reduced spatial features sets have better reliability than the current pixel shape index and length-width extraction algorithm.

According to Keaton and Brokish [4], roads extraction was performed using pan-sharpened multispectral IKONOS imagery of 1-meter spatial resolution. A semi-automated method was applied for that purpose in both urban and rural locations. Preliminary outcomes have verified the effectiveness of the algorithm for road extraction from fine spatial resolution satellite imagery with insignificant human activities. Urban expansion estimation was performed using in situ spatial data and ASTER multispectral imagery applied to the metropolitan city of Athens [5, 6]. The aim of the study was to investigate the performance of fine spatial resolution multispectral remote sensing to maintain the energy fluxes designation in urban environments. The results point out that ASTER multispectral imagery perform better in terms of understanding energy features and their effects and causes, providing an add-up to the conventional techniques for monitoring and quantification urban environments. Automated mapping of stream features was assessed using airborne multispectral remote sensing imagery, [7]. Stochastic algorithm based on the spectral angle mapping was adopted to classify tributary habitat. Results were not reliable for streambed material and water-depth mapping. Repaka et al [8] examined the classification and transportation feature extraction using two different data sets, QuickBird and IKONOS. Both pixel and object-based techniques were implemented for classification.

Mapping dry/wet snow cover has been carried out in by Gupta et al. [9] utilizing digital elevation model and IRS-LISS-III. The dry snow area and the non-melting area were found to be in robust mutual correspondence. It was found that the dry snow zone and wet snow zone possess distinctive hydrological features and can be distinguished and mapped from satellite imagery data.

Lorang et al. [10] have evaluated the geomorphic features of gravel-bed rivers by using airborne multispectral imagery. They offered an innovative quantification practice to examine the geomorphic work potential required to sustain the unstable habitat of gravel-bed river floodplains.

The aim of the current study is to assess the classification accuracies using four different classifiers and the attempt to evaluate the Stratified Mapping Process performance.

2. Material and methods

2.1. Study area

The study area, Nisos Elafonisos, is located in the Southern west of Crete and covers an area of about 4,317.21 hectares; the study area is at latitudes and longitudes of 35° 18’ 0” N, 23° 41’ 0” E, respectively (Figure 1). Human activities focus mainly on tourism are intensely affected the ecosystems in the designated study area. Therefore, Nisos Elafonisos ecosystems are fragile [11]. Wide variety of habitat types are found in the study area and generally they are under protection according to NATURA 2000.The flora is rich with few endemic species according to its geographical distribution. The rarest plant communities in the European Community is: *Ipomoea stolonifera* and *Androcymbium rechingeri*. Furthermore, the existing endemic subspecies are *Meles meles arcalus*, *Felis silvestris cretensis* and *Podarcis erhardii elaphonisii*, [12]. The study area is affected by Mediterranean weather conditions, dry hot summer and rainy cold winter. The rain season starts in October and ends in April of the next year. The dry season starts in June and ends in September of the same year. The average temperature recorded from 1972 to 2002 is about 18° C. Mean annual rainfall is about 750 mm [2].

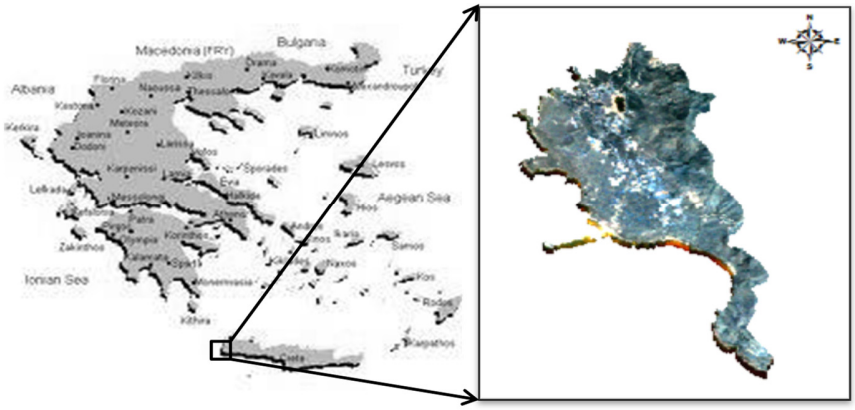


Figure 1. Location of the study area

2.2 Remote Sensing data and image prepressing

Digital sensors mounted on satellites registered the intensity of electromagnetic radiation from all locations scanned on the Earth's surface as a digital number (DN). A major characteristic of such sensors is that they record the DN for several different wavelengths of electro-magnetic energy. The exact range of DN that a sensor utilizes depends on the sensor used [5].

Radiance had to be converted to exo-atmospheric reflectance. Reflectance does not have units and is measured on a scale from 0 to 1 (or 0-100%). In order to achieve this conversion, a standardization equation was applied to every pixel in the image. This equation converts the image's digital numbers (DN, or voltage measurements) to at-sensor radiance and computes at-sensor reflectance while normalizing solar elevation angle [11]:

$$\rho_P = \frac{\pi * L_\lambda * d^2}{ESUN_\lambda * \cos\theta_S} \quad (1)$$

Where:

ρ_P is the at-satellite exo-atmospheric reflectance,

L_λ is the radiance (W m^{-2} sr^{-1} μm^{-1})

d is the earth to sun distance in astronomic units at the acquisition date

$ESUN_\lambda$ is the mean solar exo-atmospheric irradiance (W m^{-2} sr^{-1} μm^{-1}) θ_S is the solar zenith angle in degrees.

2.3 Image classification

Two approaches were tested in the current research, a pixel-based and an object-based classification approach. The pixel-based approach is represented by ML classification, one of the most popular and reliable techniques, along with a well-known machine learning method, Artificial Neural Network (ANN), and a relatively new promising algorithm, belonging to the same category, the Support Vector Machine (SVM). The object-based approach is represented by the Nearest Neighbour classifier (NN).

2.3.1 Pixel Based classification

Maximum Likelihood: uses the statistics for each class in each band as a normally distributed function and computes the likelihood of a given pixel belongs to a specific category based on the following equation:

$$g_i\,(x) = 1np(\omega_i) - {}^{1}/_{2}\ 1n|\sum i| - {}^{1}/_{2}\ (x - m_i)^T\ \sum_i^{-1}(x - \mu_i) \quad (2)$$

Where

i = class

x = n-dimensional data (where n is the number of bands)

p(ωi) = probability that class *ωi* occurs in the image and is assumed the same for all classes

|Σi| = determinant of the covariance matrix of the data in class *ωi*

Σi-1 = its inverse matrix

mi = mean vector

Artificial Neural Networks: uses standard backpropagation for supervised learning based on the following equation of [12]:

$$net_i = (x,t) = \sum_i W_{i,j}\ S_i^{'}\ (x,t) \quad (3)$$

Where

$S'_i\ (x, t)$ denotes the site attributes given by variable (neuron) *i*

$W_{i,j}$ is the weight of the input from neuron *i* to neuron *j*

$net^{j}\ (x,t)$ is the signal received for neuron *j* of cell *x* at time *t*

Support vector machine (SVM): distinguishes the categories upon margin maximization of a decision surface between the categories based on sigmoidal function equation:

$$K(x_i, x_j) = tanh(gx_i^T x_j + r\ ) \quad (4)$$

Where:

g is the gamma term in the kernel function for all kernel types except linear

r is the bias term in the kernel function for the polynomial and sigmoid kernels.

2.3.2. Object based classification

The standard Nearest Neighbour (NN) is frequently used in object-based classification, which is a non-parametric classifiers based on the absence of Gaussian distribution data model [15]. The basic concept of the NN classifier is to compute the Euclidian distance from the desired classification to the nearest training sample and assign it to that class [16]. The squared Euclidean distance is calculated following [17]:

$$distance = \sqrt{\sum_{i=1}^{n}(x_i - y_i)^2} \quad (5)$$

Where

x_i and y_i are the two locations of the desired distance.

2.3.3. Stratified Masking Process (SMP)

The SMP has been based on the calculation of the standard deviation for each class per band, in order to rank the used classes by the summation of values of the standard deviation. The ranking sequence of those values is preceded in ascending order to get the final rank, which is the base for the SMP. The results of (SMP) method are compared with the conventional classification methods using ML, ANN, and SVM classifiers. Thus, the objectives of this part of the work were to assess and compare the overall and individual accuracy as well as the kappa coefficient in order to determine the most efficient method overall as well as per-class accuracy.

2.4. Accuracy assessment

Stratified random sampling was performed to the study area to ensure that all classes were adequately represented [18]. According to Mather [19] and Niel et al. [20], a minimum of 10P to 30P pixels per class should be used for the training set, where P is the number of bands used. In the current study, random selection was made through a Sentinel-2 image with a mean of 299 pixels per class. The selection of those training sets was based on the most spectrally pure pixels per class (Table 1). Validation points were individually assigned to 16 different land cover categories according to CORINE Land Cover scheme (2006) level III. Points were used to calculate user's, producer's and overall accuracies. Producer's accuracy is calculated as following:

$$\text{Producer accuracy} = \frac{C_{aa}}{C_{*a}} X100\% \quad (6)$$

Where,

C_{aa} is element at position ath row and ath column

C_{*a} is column sums

User's accuracy is calculated as following:

$$\text{User accuracy} = \frac{C_{ii}}{C_{i*}} X100\% \quad (7)$$

C_{ii} is element at position ath row and ath column

C_{i*} is row sums

Overall accuracy is calculated as following:

$$\text{User accuracy} = \frac{\sum_{a=1}^{U} C_{aa}}{Q} X100\% \quad (8)$$

Where,

Q and U is the total number of pixels and classes respectively.

Matching of user's and producer's accuracies delivers accurateness to the classification and assures a robust liability of the implemented accuracy assessment ([13, 14].

K_{hat} statistics is a second measure accuracy agreement. This measure of agreement is based [4] (1983) findings. K_{hat} was calculated using the following equation:

$$\mathrm{K}_{hat} = \frac{N \cdot \sum_{i=1}^{r} x_{ii} - \sum_{i=1}^{r} \left(x_{ij} \cdot x_{ji} \right)}{N^2 - \sum_{i=1}^{r} \left(x_{ij} \cdot x_{ji} \right)} \quad (9)$$

Where

r, number of rows in the error matrix;

x_{ii}, number of observations in row i and column i (the diagonal cells);

x_{i+}, total observations of row i;

x_{+I}, total observations of column i,

N, total of observations in the matrix.

Table 1. Validation and training point distribution among classes.

Classes	Validations points		Training points
	Identified via image analysis	Identified via points from the field	
AL	62	4	462
BDS	9	2	61
BR	82	2	658
CUF	114	2	920
DUF	20	2	77
GUA	8	7	75
HAA	83	2	191
MES	20	2	85
NG	46	12	333
OG	69	15	457
P	5	2	15
PA	5	2	75
SH	6	2	164
SO	0	2	219
SV	150	23	684
SVA	290	8	395
Total	969	89	
Final Total	**1058**		**5041**

Where

AL = Arable Land, **BDS** = Beaches, Dunes and Sands, **BR** = Bare Rocks, **CUF** = Continuous Urban Fabric, **DUF** = Discontinuous Urban Fabric, **GUA** = Green Urban Area, **HAA** = Heterogeneous Agricultural Areas, **MES** = Mineral Extraction Sites, **NG** = Natural Grasslands, **OG** = Olive Groves, **P** = Pastures, **PA** = Port Areas, **SH** = Scrub/Herbaceous, **SO** = Sea and Ocean, **SV** = Sclerophyllous Vegetation and **SVA** = Sparsely Vegetated Areas.

3. Results and discussion

The use of ML, ANN, NN and especially SVM classifiers in LU/LC mapping for Mediterranean fragmented landscape is very significant, given that the validation data's choice was based on the ground truth data collection throughout several field visits. Table 2 shows the accuracy assessment results for the four classifiers with the producer's and user's accuracy, as well as overall accuracy and kappa coefficients. The resulting maps from ML, ANN, SVM, and NN in object-based classification are shown in Figures 2, 3, 4 and 5 respectively. According to the results, SVM has performed better overall in comparison to the OBIA (NN), ANN, and ML classifiers.

The SVM classifier achieved the highest accuracy among other classifiers, by taking into account the good agreement, proved by the kappa coefficient (K) value, and the number of classes segregated successfully in both user and producer accuracies. Higher classification accuracies were noted for "Agricultural areas", then for Forest and Semi Natural Areas (FSNA), and finally for the Artificial Surface (AS). However, SVM failed to perform accurately classes like Pasture (P), a fact which may be due to the inability of SVM to transform non-linear decision boundaries in a high dimensional space, in the case of low training-site number. Class P is represented by a few sparse patches within the study AREA [21]. The same results were noticed with ANN. OBIA (NN) and ML, however, succeeded to demonstrate better classification results in this case.

OBIA (NN) performed better than either of the other classifiers, ANN and ML as shown in Table 2, with a good agreement overall. In addition, it succeeded to discriminate artificial surfaces successfully with the highest accuracy overall. Moreover, Sparsely Vegetated Areas (SVA), Bare Rock (BR), and Natural Grassland (NG) classes belonging to the FSNA class were successfully discriminated by OBIA (NN) compared to the other classifiers, which shows the potential of the method to benefit from the extra added layers, especially LAI, in order to set apart FSNA subclasses. However, OBIA (NN) failed to

classify Green Urban Areas (GUA) class, which may be due to the inability of the classifier to separate that class spectrally. The field visit proved that GUA and Sclerophyllous vegetation (SV) classes consist of similar vegetation types, which could be the main reason for their confusion, [1].

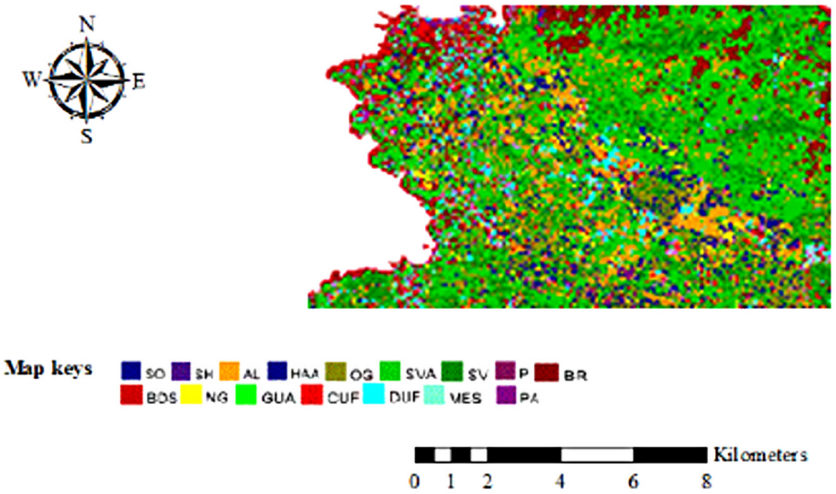


Figure 2. ML classification result using Sentinel-2 imagery

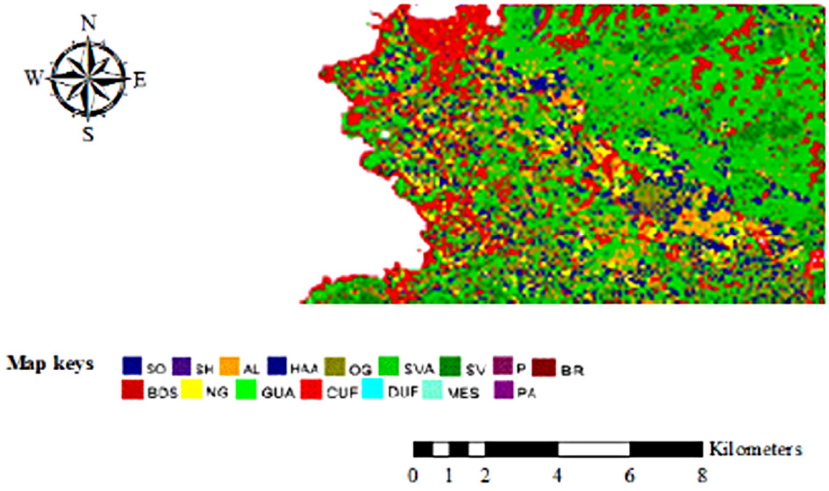


Figure 3. ANN classification result using Sentinel-2 imagery

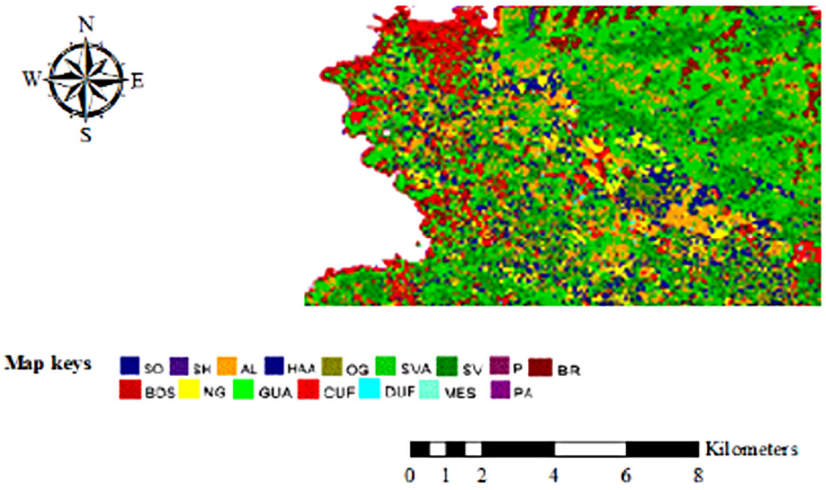


Figure 4. SVM classification result using Sentinel-2 imagery

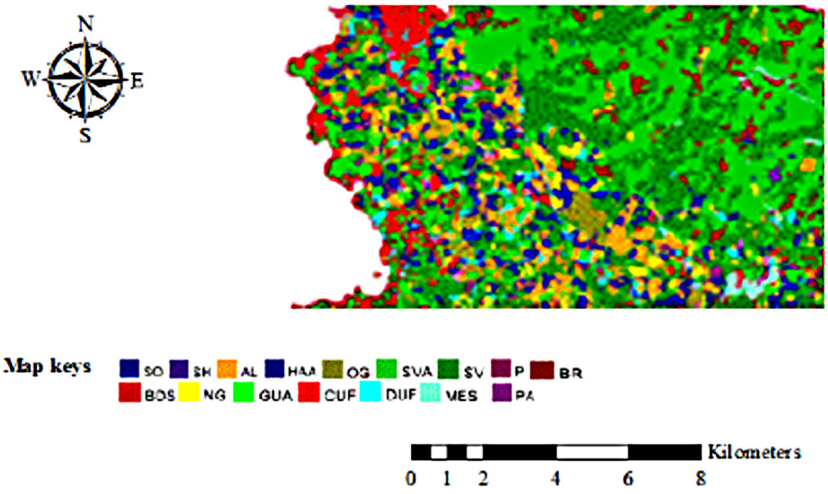


Figure 5. OBIA (NN) classification result using Sentinel-2 imagery

Meanwhile, the SMP method did not succeed to overcome the conventional classification method using the ML and SVM classifiers. ML performs better that the SMP method with quite a big margin between the results of the overall accuracy and kappa coefficient. However, the differences between the conventional classification method and SMP were not so robust when SVM was used applying the Radial Basic Function (RBF) kernel with almost 3% difference in the overall accuracy and less than 1% for the kappa coefficient. Hence, the well-known ML classifier, using the traditional method, performs better than SVM in both cases, with 78.05% and 0.6342 for the overall accuracy and K, respectively. SA, BR and HAA classes were the most failure classes to distinguish as it's illustrated in Figures 6, 7 and 8.

Table 2. Accuracy assessment results from the four classifiers

	ML		SVM		ANN		OB-NN	
Class	**Prod.Acc**	**User.Acc**	**Prod.Acc**	**User.Acc**	**Prod.Acc**	**User.Acc**	**Prod.Acc**	**User.Acc**
AL	82.32	78.68	100	95.19	69.82	96.72	100	83.12
BDS	100	48.44	100	76.07	100	46.52	76.07	55.62
BR	80.36	60.48	93.84	88.57	96.25	74.22	93.84	89.58
CUF	25.42	53.9	95.85	70.5	95.85	63.36	95.85	70.06
DUF	26.07	20.3	16.07	100	0	0	76.07	89.31
GUA	39.53	56.63	47.22	86.78	0	0	0	0
HAA	40.83	65.78	75.77	87.18	80.59	59.48	96.25	55.55
MES	81.07	28.19	41.07	100	41.07	10	76.07	89.31
NG	54.64	63.57	88.57	72.08	55.62	52.79	86.78	91.64
OG	81.56	63.33	93.75	91.55	93.75	57.37	99.85	91.07
P	17.74	8.76	0	0	0	0	100	51.07
PA	100	16.7	61.07	100	8.07	21.07	61.07	100
SH (SVA)	100	100	100	86.78	100	86.78	84.4	56.63
SV	65.98	86.45	94.05	96.28	45.51	97.27	82.94	67.42
SVA	83.16	82.89	96	95.05	82.83	81.74	46	97.45
Overall	**65.82%**		**88.42%**		**73.07%**		**77.05%**	
Kappa	**0.6938**		**0.8821**		**0.6716**		**0.7381**	

Looking closely at the performance of SMP, it was noticed that in some classes that the conventional classification output per class and that of the SMP method gave inconsistent results. Figure 6 below shows that the AS classification results generated from both classifiers are different, but when compared to the SMP method output, it produced the same results. However, this wasn't the case with the BR class as well as HAA (Figure 7 and 8). Application of SMP has different classification results before and after the application of the SMP method for both classifiers. In fact, the difference is quite noticeable between both methods, even when visual analysis is performed. This is interesting for the performance of the SMP method since it should omit the irrelevant pixels for each used class in the classification procedure.

The classification accuracy was performed over the entire image using the same training sites and validated using the same testing points for all classifiers. The differences between SVM and the other classifiers are quite significant due to its capability of locating an optimal separating hyperplane, since the design of the classifiers is quite different, which concords with Kavzoglu and Colkesen [22]. Using Landsat ETM+ and Terra ASTER images, applied in Turkey (Gebze district), they recorded better performance of SVM using the RBF kernel over the ML classifier, in terms of overall and per class accuracies. Comparable results were recorded by Elhag et al. [21] using SVM, ML and ANN and the Decision-Tree Classifier (DTC) applied on Landsat ETM+ data acquired in Nile Delta.

For the conventional method using the ML classifier, the overall accuracy was 71.27% and the kappa coefficient was 0.652. The highest accuracy was registered in the SH (SVA) class while the lowest was in the OG class with 44% for user accuracy. However, the overall accuracy of the SMP method was 50.57%, with kappa coefficient of 0.38, generating a low agreement with the reference points. The lowest accuracy was registered in the HAA class with 14.81% and the highest was in the AL class with 97.96% after the SH (SVA) class with 100%. Confusion was noticed in the HAA class with the SHVA class generating a big commission error. Similar results were noticed with the SVA and SHVA classes caused by the closer values of spectral reflectance. The AS and BR classes have the same problem of similarity in spectral reflectance. Even with a careful selection of the training site, the problem remains. Thus, except for AL, all the other classes in the second level suffer from omission and commission errors.

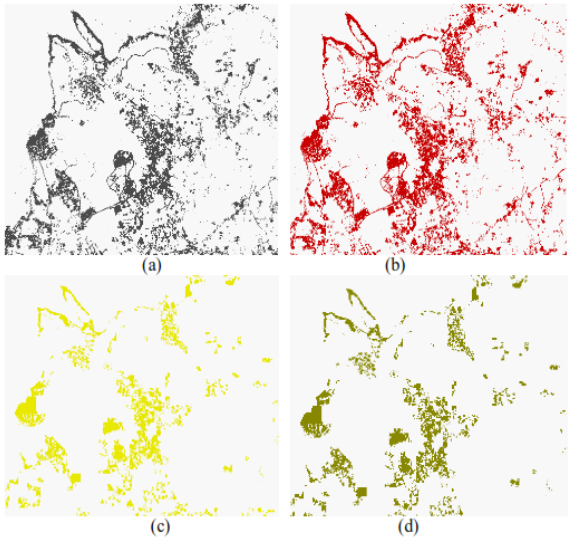


Figure 6. A subset comparison of classification images from the ML (a, b) and SVM (c, d) classifiers for the AS class (Level 1); (a) and (c) before the application of SMP method and (b) and (d) after

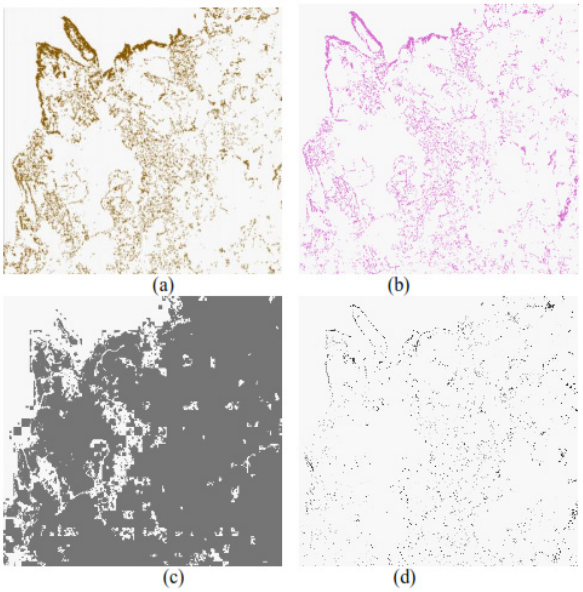


Figure 7. A subset comparison of classification images from the ML (a, b) and SVM (c, d) classifiers for the BR class (Level 2); (a) and (c) before the application of SMP method and (b) and (d) after

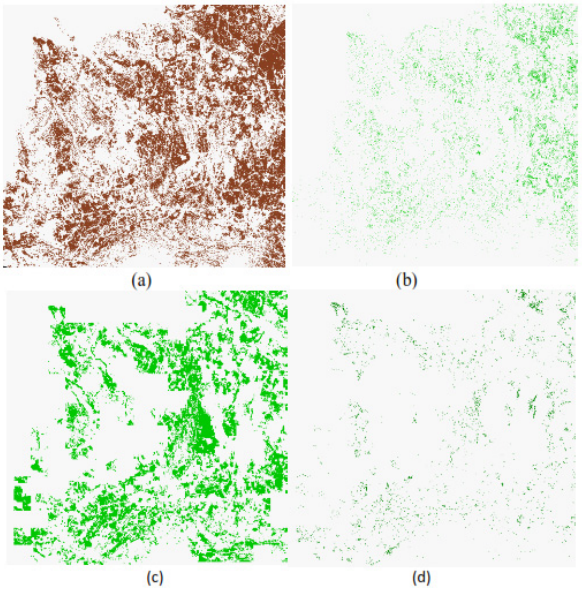


Figure 8. A subset comparison of classification images from the ML (a, b) and SVM (c, d) classifiers for the HAA class (Level 2); (a) and (c) before the application of SMP method and (b) and (d) after

For the SVM classifier under the SMP method, the accuracy results were almost the same with 51.63% overall accuracy and 0.375 for the kappa coefficient. The weakest results were in the OG class with 92.16% user accuracy and the highest was in the SH (SVA) class with 100%. Commission errors were registered widely in the HAA, AS and less accentuated in BR. Still, the BR class has a big omission with the SVA class. This confusion comes from the mix of shrubs and rocks on the ground, especially when the vegetation is quite sparse and little, which generates a similar spectral signature. The SVA class has quite a distributed omission error with all the classes except the SH (SVA) class while the largest one was registered with SHVA. Similar results were registered with the OG class.

4. Conclusions

Pixel-based and object-based approaches were used for the classification of the Sentinel-2 image. The pixel-based approach holds three classifiers, namely: Maximum Likelihood, Artificial Neural Network, and Support Vector Machine, with the implementation of the new method, Stratified Mapping Process, which was applied using the Maximum Likelihood and Support Vector Machine classifiers. Maximum Likelihood produced the highest accuracy for the Pasture class in terms of individual class identification, which was the output of a larger spectral range of the selected training pixel, allowing the Maximum Likelihood classifier to define larger decision regions for these particular classes. Support Vector Machine succeeded to distinguish with high accuracy most of the classes which makes it the best overall in terms of individual identification accuracy. Object Based Image Analysis (Nearest Neighbour) has succeeded in segregating individual classes of the Artificial Surfaces with success more than any other classifier. Only Nearest Neighbour succeeded to fully classify that class within the other classifiers. In both classifiers, Support Vector Machine and Artificial Neural Network, the Artificial Surfaces class is confused with the Continuous Urban Fabric class, but for Maximum Likelihood the confusion was with the Discontinuous Urban Fabric class and Port Areas classes. The testing of the Stratified Mapping Process method didn't generate good results compared to the conventional classification method. The fragmented patchy study

area confuses the classifier by generating more commission and omission errors when compared to a normal place where each class occupies a big area with clearly distinguished classes.

Acknowledgement
This article was funded by the Deanship of Scientific Research (DSR) at King Abdulaziz University, Jeddah. The authors, therefore, acknowledged with thanks DSR for technical and financial support.

References

[1] Elhag, M., 2016a. Quantification of Land Cover Changes Based on Temporal Remote Sensing Data for Ras Tarout Area, Saudi Arabia. Indian Journal of Geo-Marine Sciences, paper accepted and undergoes publishing
[2] Elhag, M., 2016b. Evaluation of Different Soil Salinity Mapping Using Remote Sensing Techniques in Arid Ecosystems, Saudi Arabia. Journal of Sensors, 2016: 96175-96175
[3] Huang, C. M., Lee, Y. J., Lin, D. K. J., Huang, S. Y., 2007. Model selection for support vector machines via uniform design. Computational Statistics and Data Analysis, 52: 335 – 346
[4] Keaton, T., Brokish, J., 2002. A Level Set Method for the Extraction of Roads from Multispectral Imagery. Proceedings 31st for Applied Imagery Pattern Recognition Workshop, Washington DC, USA, 141–147
[5] Boyd, D. S., Duane, W. J., 2001. Exploring spatial and temporal variation in middle infrared reflectance (at 3.75 μm) measured from the tropical forests of West Africa. International Journal of Remote Sensing, 22: 1861−1878
[6] Chrysoulakis, N., 2003. Estimation of the All-Wave Urban Surface Radiation Balance by use of ASTER Multispectral imagery and in Situ Spatial Data. Journal of Geophysical Research, 108: 4582-4592
[7] Leckie, D. G., Jay, Ed-C. C., Paradine, D., 2005. Automated Mapping of Stream Features with High-Resolution Multispectral Imagery: An Example of the Capabilities. Photogrammetric Engineering and Remote Sensing, 71:145–155
[8] Repaka, S. R., Truax, D. D., Kolstad, E., Hara, C. G. O., 2004. Comparing Spectral and Object Based Approaches for Classification and Transportation Feature Extraction from High Resolution Multispectral Imagery. Photogrammetric Engineering and Remote Sensing, 45: 212-218
[9] Gupta, R. P., Haritashya, U. K., Singh, P., 2005. Mapping Dry/Wet Snow Cover in the Indian Himalayas Using IRS Multispectral Imagery. Remote Sensing of Environment, 97: 458-469
[10] Lorang, M. S., Whited, D. C., Hauer, F. R., Kimball, J. S., Stanford, J. A., 2005. Using Airborne Multispectral Imagery to Evaluate Geomorphic Work Across Flood Plains of Gravel Bed River. Ecological Applications, 15:1209–1222
[11] Elhag, M., 2011. Land Suitability for Afforestation and Nature Conservation Practices Using Remote Sensing & GIS Techniques. Catrina Journal, 6(1): 11–17
[12] Soupios, P., Papadopoulos, I., Kouli, M., Georgaki, I., Vallianatos, F., Kokkinou, E., 2007. Investigation of Waste Disposal Areas Using Electrical Methods: A Case Study from Chania, Crete, Greece. Environmental Geology, 51: 1249–1261
[13] Richards, J., 1999. Remote Sensing Digital Image Analysis, Springer-Verlag, Berlin, P. 240-280.
[14] Okwuashi, O., Isong, M., Eyo, E., Eyoh, A., Nwanekezie, O., Olayinka, D. N., Udoudo, D. O., Ofem, B., 2012. GIS Cellular Automata Using Artificial Neural Network for Land-use Change Simulation of Lagos, Nigeria. Geography and Geology, 4(2): 94-101
[15] Hubert-Moy, L., Quêté, Y., Billot, M., Corgne, S., 2001. Trajectories of Land-cover-change in intensive agricultural regions: a short-time predictive approach with the Dempster-Shafer theory,

First International Workshop on the Analysis of Multi-temporal Remote Sensing images, September 13-14

[16] Keller, J. M., Gray, M. R., Givens, J. A., 1985. A Fuzzy K-Nearest Neighbor Algorithm. IEEE Transaction on System Management and Cybernetics, 15: 580-585

[17] Varma, M., Zisserman, A., 2005. Unifying statistical texture classification frameworks. International Journal of Computer Vision, 62(1/2): 61–81

[18] Knight, J. F., 2002. Accuracy Assessment of Thematic Maps Using Interclass Spectral Distances, Dissertation in partial fulfillment for PhD, North Carolina State University, 110 p.

[19] Mather, P., 2004. Computer Processing of Remotely-Sensed Images: An Introduction (3rd Ed), New York: John Wiley & Sons Press, ISBN: 978-0-470-84919-4.

[20] Niel, V., McVicar, T. G., Datt, T. R., 2005. On the Relationship Between Training Sample Size and Data Dimensionality of Broadband Multi-temporal Classification. Remote Sensing of Environment, 98:468–480

[21] Elhag, M., Psilovikos, A., Sakellariou, M., 2013. Detection of Land Cover Changes for Water Recourses Management Using Remote Sensing Data over the Nile Delta Region. Environment, Development and Sustainability, 15(5): 1189-1204

[22] Kavzoglu, T., Colkesen, I., 2009. A kernel Functions Analysis for Support Vector Machines for Land Cover Classification. International Journal of Applied Earth Observation and Geoinformation, 11: 352–359.